

Nonclassical photocounting statistics with a single on-off detector

V. S. Kovtoniuk ,¹ M. Bohmann ,² and A. A. Semenov ,^{1,3,4}

¹*Bogolyubov Institute for Theoretical Physics, National Academy of Sciences of Ukraine,
Vulytsya Metrolohichna 14-b, 03143 Kyiv, Ukraine*

²*Quantum Technology Laboratories GmbH, Clemens-Holzmeister-Straße 6/6, 1100 Vienna, Austria*

³*Department of Theoretical and Mathematical Physics,
Kyiv Academic University, Boulevard Vernadskogo 36, 03142 Kyiv, Ukraine*

⁴*Department of Mathematics, Kyiv School of Economics, Vulytsya Mykoly Shpaka 3, 03113 Kyiv, Ukraine*

Any single on-off photocounter, which can only detect the presence or absence of photons without discriminating their number, is not capable of identifying nonclassical nature of light. This limitation arises because any photocounting statistics obtained with such a detector can be easily reproduced with coherent states of a light mode. We show that a simple modification of an on-off detector—introducing controlled attenuation as a tunable setting—enables such detectors to reveal nonclassical properties of radiation fields.

I. INTRODUCTION

The concept of nonclassical states in quantum optics [1–9] derives from the observation that all measurements on coherent states and their statistical mixtures can be explained within the framework of classical electrodynamics. Technically, it is related to the Glauber-Sudarshan P representation [10, 11]. It establishes that the density operator $\hat{\rho}$ of an electromagnetic field mode can be expanded by projectors of coherent states $|\alpha\rangle$,

$$\hat{\rho} = \int_{\mathbb{C}} d^2\alpha P(\alpha) |\alpha\rangle\langle\alpha|, \quad (1)$$

where $P(\alpha)$ is the Glauber-Sudarshan P function. If $P(\alpha) \geq 0$, i.e. it can be interpreted as a probability distribution, then the corresponding quantum state is classical. All states that violate this condition are considered in quantum optics as nonclassical. Optical nonclassicality encompasses a number of nonclassical phenomena such as photon-number [12] and quadrature [13–17] squeezing and their further generalizations to higher-order nonclassical effects [18]. Moreover, a number of techniques have been developed to detect and quantify optical nonclassicality; see, e.g., Refs. [19–50].

Optical nonclassicality is often considered in the framework of quantum resource theories [51, 52]. Indeed, nonclassicality can be interpreted as a generalization of quantum coherence [7, 53]. In particular, nonclassicality is a resource in quantum metrology [54, 55], quantum linear networks such as boson-sampling schemes [56], quantum kernel methods [57], and so on. Importantly, optical nonclassicality is the resource for generating quantum entanglement with passive linear optical elements [26, 39].

Experimentally accessible information about a given quantum state of light is encoded in measurement statistics. In typical scenarios, this information is not complete to reconstruct the density operator of the studied quantum state. Counting of photons represent a typical example of such informationally-incomplete measurements. In this case, the photocounting probability distribution

$\mathcal{P}(n)$ is given by

$$\mathcal{P}(n) = \text{Tr} \left[\hat{\rho} \hat{\Pi}(n) \right], \quad (2)$$

where $\hat{\Pi}(n)$ is the positive operator-valued measure (POVM). For ideal photon-number resolving detection the POVM is known from the photodetection theory [3, 58]. In more realistic scenarios, it may differ significantly from this ideal situation [59–62].

By substituting Eq. (1) into Eq. (2), we can rewrite the latter in the P representation [63, 64],

$$\mathcal{P}(n) = \int_{\mathbb{C}} d^2\alpha P(\alpha) \Pi(n|\alpha), \quad (3)$$

where $\Pi(n|\alpha) = \langle\alpha| \hat{\Pi}(n) |\alpha\rangle$ is the photocounting probability distribution for the coherent state $|\alpha\rangle$. If the state $\hat{\rho}$ is classical, i.e., if $P(\alpha) \geq 0$, then $\mathcal{P}(n)$ can be sampled from the statistical mixture of coherent states. However, if we treat Eq. (3) as an integral equation in $P(\alpha)$ for a given $\mathcal{P}(n)$ and $\Pi(n|\alpha)$, we observe that it may yield multiple solutions due to informational incompleteness. If at least one of these solutions is non-negative, then $\mathcal{P}(n)$ can be sampled from a statistical mixture of coherent states even if the state $\hat{\rho}$ is nonclassical [45–49].

This situation is always inherent to on-off detectors, which can only detect the presence or absence of electromagnetic radiation without distinguishing between the number of photons. The POVM of these detectors is easily obtained from the POVM of ideal photon-number resolving detectors [3, 58]. The corresponding photon-number distribution for the coherent state $|\alpha\rangle$ is given by

$$\Pi(0|\eta; \alpha) = \exp(-\eta|\alpha|^2), \quad (4)$$

$$\Pi(1|\eta; \alpha) = 1 - \Pi(0|\eta; \alpha). \quad (5)$$

Here $n = 0$ and $n = 1$ correspond to the case of no click and click, respectively, and $\eta \in [0, 1]$ is the detection efficiency. Obviously, any photocounting statistics obtained from such a detector can always be reproduced by a coherent state whose amplitude satisfies

$|\alpha|^2 = -\ln \mathcal{P}(0)/\eta$. This is the reason why on-off detectors are not considered capable of detecting nonclassicality of quantum states.

In this paper, we show that a simple modification of on-off detectors makes it possible to detect nonclassicality of photocounting statistics. Moreover, our technique works even for counterintuitive examples where the photocounting statistics obtained with ideal photon-number resolving detectors are super-Poissonian. The result can be achieved by treating the detection efficiency η as a device setting that takes on a discrete, finite set of N values η_i , $i = 1 \dots N$, such that $\eta_1 < \eta_2 < \dots < \eta_N$. In experiments, this is easily implemented by placing an amplitude modulator in front of the detector, see Fig. 1. In this case, the detection of nonclassicality is reformulated as a test for the impossibility of reproducing the set of no-click probabilities

$$\mathcal{P}(0|\eta_i) = \text{Tr} \left[\hat{\rho} \hat{\Pi}(0|\eta_i) \right], \quad (6)$$

for the state $\hat{\rho}$ with a statistical mixture of coherent states. This formulation does not include the probabilities $\mathcal{P}(1|\eta_i)$, since they depend on $\mathcal{P}(0|\eta_i)$ according to Eq. (5).



FIG. 1. The scheme of experiment for detecting nonclassicality of photocounting statistics with an on-off detector. The detector is preceded by an amplitude modulator, whose transmittance may take the values η_i , $i = 1 \dots N$.

A similar task for general measurements has been considered in Refs. [45, 49], see also Refs. [28, 46–48] for important examples. In particular, as discussed in Ref. [49], there are inequalities that tightly bound a convex set of classical probability distributions. Violation of these inequalities is a necessary and sufficient condition for optical nonclassicality of measurement statistics and a sufficient condition for optical nonclassicality of quantum states. In this paper, we apply this technique to reveal nonclassicality of photocounting statistics obtained with a single on-off detector having switchable detection efficiency.

The rest of the paper is organized as follows. In Sec. II, we introduce the general framework for constructing tight inequalities that reveal nonclassicality with the device under consideration. Intuitive cases with two and three settings are considered in Sec. III. Complete sets of tight inequalities for an arbitrary number of settings are derived in Sec. IV. An alternative technique leading to inequalities nonlinear with respect to the probabilities $\mathcal{P}(0|\eta_i)$ for $\eta_i = i/N$ is introduced in Sec. V. Applications of our approach to squeezed coherent states are consid-

ered in Sec. VI. Summary and concluding remarks are given in Sec. VII.

II. TIGHT INEQUALITIES REVEALING NONCLASSICALITY

In this section we remind the reader with tight inequalities for nonclassicality of measurement statistics introduced in Ref. [49], see also Ref. [48], and discuss the background of tailoring this method to the case considered in this paper. It is particularly useful to use the geometric picture of this technique from the very beginning of our consideration. Observe that all coherent-state probability distributions $\Pi(0|\eta; \alpha)$ depend on the magnitude of the coherent amplitude α and not on its phase. This implies, we can employ a useful reparameterization by introducing a new parameter

$$t = \exp(-\eta_1|\alpha|^2), \quad (7)$$

where η_1 is the lowest efficiency among all η_i . Then Eq. (4) is reduced to the form

$$\Pi(0|\eta; t) = t^{\eta/\eta_1}, \quad (8)$$

where $t \in [0, 1]$. Considering N settings $\eta = \eta_i$, where $i = 1 \dots N$, we introduce the new vector

$$\mathbf{\Pi}(t) = (\Pi_1(t) \ \Pi_2(t) \ \dots \ \Pi_N(t))^T, \quad (9)$$

composed of the components

$$\Pi_i(t) = \Pi(0|\eta_i; t) \quad (10)$$

and parameterized by the parameter t . Similarly, we define the vector

$$\mathbf{\mathcal{P}} = (\mathcal{P}_1 \ \mathcal{P}_2 \ \dots \ \mathcal{P}_N)^T, \quad (11)$$

whose components

$$\mathcal{P}_i \equiv \mathcal{P}(0|\eta_i) \quad (12)$$

are the no-click probabilities given by Eq. (6).

The vector $\mathbf{\mathcal{P}}$ (the set of no-click probabilities) can be reproduced with classical electromagnetic fields if there exists such $\varrho(t) \geq 0$ that

$$\mathbf{\mathcal{P}} = \int_0^1 dt \varrho(t) \mathbf{\Pi}(t). \quad (13)$$

For classical states, $\varrho(t)$ can be directly derived from a non-negative P function of the state. However, it can also exist for nonclassical states, due to informational incompleteness of the measurement procedure.

The set $\mathcal{C} = \{\mathbf{\Pi}(t) | t \in [0, 1]\}$ defines a closed curve in the N -dimensional Euclidean space of the vectors $\mathbf{\mathcal{P}}$. Then Eq. (13) states that the vector $\mathbf{\mathcal{P}}$ can be reproduced by classical radiation fields if and only if it belongs to the

convex combination of the set \mathcal{C} , $\mathcal{H} = \text{Conv} \mathcal{C}$. Applying to this statement the hyperplane supporting theorem [65] and the methods of Refs. [45, 49, 66], we conclude that the vector \mathcal{P} is classically treatable if and only if for any vector λ the inequality

$$\lambda \cdot \mathcal{P} \leq \sup_{t \in [0,1]} \lambda \cdot \Pi(t) \quad (14)$$

is satisfied. If we find at least a single instance of λ such that this inequality is violated, then the vector \mathcal{P} (the set of all no-click probabilities) cannot be reproduced with the statistical mixtures of coherent states.

A straightforward way to deal with this problem may be to apply an optimization procedure to find vectors λ that violate inequality (14). However, we can significantly reduce computational resources, by optimizing the set of λ . This optimal set Λ corresponds to the set of tight inequalities [49], which (1) can be used to derive any other inequality outside this set and (2) are independent, i.e. no tight inequality can be derived from other tight inequalities. As discussed in Ref. [49], the vectors λ corresponding to tight inequalities are normal vectors to the supporting hyperplanes of the manyfold \mathcal{H} .

Each supporting hyperplane should include at least one point of the curve \mathcal{C} . For each value t_1 of the parameter t , we can define a set of vectors $\lambda(t_1)$ that form closed convex cones,

$$L(t_1) = \left\{ \lambda(t_1) \mid \arg \max_{t \in [0,1]} \lambda(t_1) \cdot \Pi(t) = t_1 \right\}. \quad (15)$$

In the considered scenario it is possible for a single value of t_1 to be associated with multiple values of $\lambda(t_1)$. Independent vectors $\lambda(t_1)$ correspond to extreme rays $\text{Ext}[L(t_1)]$. Finally, the set

$$\Lambda = \bigcup_{t_1 \in [0,1]} \text{Ext}[L(t_1)] \quad (16)$$

defines all vectors $\lambda(t_1)$ that generate tight inequalities. The application of this method to the photocounting problem, where the vector \mathcal{P} represents a photocounting statistic, have been derived in Ref. [49]. The same procedure is straightforwardly generalized to the scenario where the vector \mathcal{P} represents the no-click probabilities considered in this paper.

III. TWO AND THREE SETTINGS

We start our analysis with the intuitively accessible cases of $N = 2$ and $N = 3$. In these scenarios, the curve \mathcal{C} and its convex hull \mathcal{H} can be easily visualized, providing clear geometric insight into the structure of the problem. These simple examples serve as a useful foundation for understanding the general approach developed in the following sections. Here, we focus on an intuitive understanding of the results, while deferring a more rigorous derivation, which is applicable to arbitrary N , to the next section.

A. Two settings

In the case of $N = 2$, Eq. (8) reduces to

$$\Pi_1(t) = t, \quad (17)$$

$$\Pi_2(t) = t^{\nu_2}, \quad (18)$$

where $\nu_2 = \eta_2/\eta_1$. Therefore, the curve \mathcal{C} is described by the equation

$$\mathcal{P}_2 = \mathcal{P}_1^{\nu_2}, \quad (19)$$

see Fig. 2. Since $\nu_2 > 1$, its convex hull \mathcal{H} is clearly the region bounded by this curve and the line $\mathcal{P}_2 = \mathcal{P}_1$.

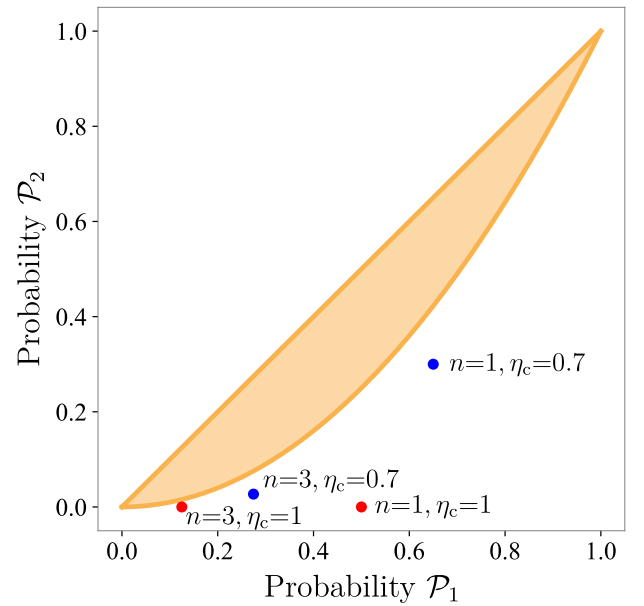


FIG. 2. Classical region for $N = 2$ settings (shaded), its boundary (solid line), and points related to the Fock states $|n\rangle$ attenuated with the efficiency η_c . In this example, $\eta_1 = 1/2$ and $\eta_2 = 1$.

We now proceed to examine this construction in more technical detail. According to Eq. (15), at each point $t_1 \in (0,1)$, the vectors $\lambda(t_1)$ defining tight inequalities satisfy the equation

$$\lambda(t_1) \cdot \dot{\Pi}(t_1) = 0, \quad (20)$$

where the overdot denotes differentiation. Clearly, its solution yields the maximum of $\lambda(t_1) \cdot \Pi(t)$ with respect to t at the point $t = t_1$. It is given by

$$\lambda(t_1) = \begin{pmatrix} \dot{\Pi}_2(t_1) \\ -\dot{\Pi}_1(t_1) \end{pmatrix} = \begin{pmatrix} \nu_2 t_1^{\nu_2} \\ -1 \end{pmatrix}. \quad (21)$$

The vectors $\lambda(t_1)$ are normal to the tangent line of the curve (19), which are supporting hyperplanes of \mathcal{H} . Similar to the scenario described in Ref. [49], at the endpoints of this curve, $t = \tau \in \{0,1\}$, condition (15)

defines the conic combinations of the vectors $\lambda(\tau)$ and $\lambda_\prec = (-1 \ 1)^\top$. Therefore, according to Eq. (16) the complete set of tight inequalities is given by the vectors $\lambda(t) \in [0, 1]$ and λ_\prec .

The set of linear tight inequalities can be combined into two nonlinear inequalities,

$$\mathcal{P}_1^{\nu_2} \leq \mathcal{P}_2, \quad (22)$$

$$\mathcal{P}_2 \leq \mathcal{P}_1 \quad (23)$$

related to $\lambda(t) \in [0, 1]$ and λ_\prec , respectively. In fact, they define the convex set \mathcal{H} of the curve \mathcal{C} given by Eq. (19), cf. Fig. 2. Besides, inequality (23) represents the trivial fact that the no-click probability with efficiency η_1 is higher than the same probability with efficiency η_2 for $\eta_1 < \eta_2$.

This elementary case of $N = 2$ is already suitable to reveal nonclassicality of the Fock states $|n\rangle$, attenuated with the efficiency η_c . For these states, inequality (22) is reduced to the inequality $(1 - \eta_1 \eta_c)^{n\nu_2} \leq (1 - \eta_2 \eta_c)^n$, which is always violated. As shown in Fig. 2, all points related to the attenuated Fock states are placed outside the set \mathcal{H} .

B. Three settings

In the case of $N = 3$, Eq. (8) is given by

$$\Pi_1 = t, \quad (24)$$

$$\Pi_2 = t^{\nu_2}, \quad (25)$$

$$\Pi_3 = t^{\nu_3}, \quad (26)$$

where $\nu_i = \eta_i/\eta_1$ such that $1 < \nu_2 < \nu_3$. These equations parametrically define the curve \mathcal{C} in a three-dimensional space. Our task is to construct the convex hull \mathcal{H} of this curve. Appropriate mathematical methods to solve this problem are described in Refs. [67–69]. We use the idea of Ref. [49] to obtain this result in an intuitively clear way.

Let t_1 be the value of the parameter t at which $\lambda \cdot \Pi(t)$ attains its maximum with respect to t . Clearly, a supporting hyperplane of \mathcal{H} that contains the point $\Pi(t_1)$ is parallel to the vector $\dot{\Pi}(t_1)$, which is tangent to the curve \mathcal{C} at $t = t_1$. We also assume that each point t_1 corresponds to two supporting planes, each passing through one of the endpoints $\Pi(\tau)$, where $\tau = 0$ or $\tau = 1$. Hence, the vectors λ also depend on the parameter τ . These vectors, normal to the supporting plane and directed outward from \mathcal{H} , are given by

$$\lambda(t_1; \tau) = \mathcal{N}(-1)^{1+\tau} \dot{\Pi}(t_1) \times \Delta\Pi(\tau, t_1), \quad (27)$$

where

$$\Delta\Pi(t', t'') = \Pi(t') - \Pi(t''), \quad (28)$$

see Fig. 3.

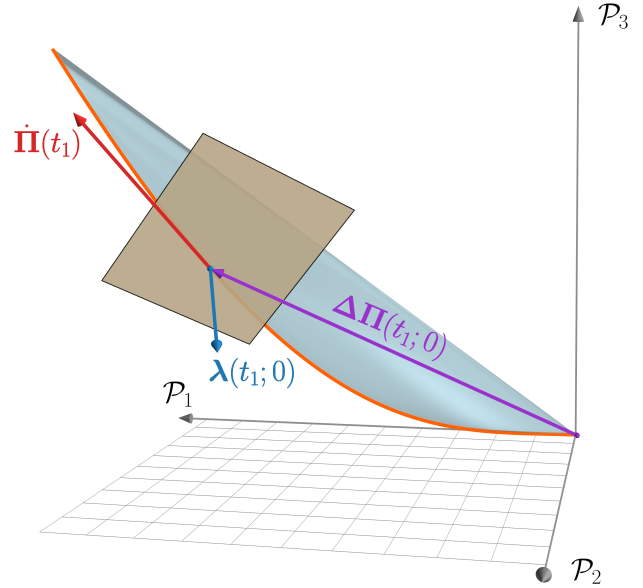


FIG. 3. The curve \mathcal{C} and its convex hull \mathcal{H} for the case of $N = 3$. Also the vectors $\lambda(t_1; \tau)$ and the vectors $\Delta\Pi(t_1, 0)$ and $\dot{\Pi}(t_1)$ defining supporting planes of \mathcal{H} are shown for $\tau = 0$.

The explicit form of the vectors $\lambda(t_1; \tau)$,

$$\lambda(t_1; 0) = \mathcal{N} \begin{pmatrix} -(\nu_3 - \nu_2) t_1^{\nu_2 + \nu_3 - 1} \\ (\nu_3 - 1) t_1^{\nu_3} \\ -(\nu_2 - 1) t_1^{\nu_2} \end{pmatrix}, \quad (29)$$

$$\lambda(t_1; 1) = \mathcal{N} \times \begin{pmatrix} (\nu_3 - \nu_2) t_1^{\nu_3 + \nu_2 - 1} - \nu_3 t_1^{\nu_3 - 1} + \nu_2 t_1^{\nu_2 - 1} \\ -(\nu_3 - 1) t_1^{\nu_3} + \nu_3 t_1^{\nu_3 - 1} - 1 \\ (\nu_2 - 1) t_1^{\nu_2} - \nu_2 t_1^{\nu_2 - 1} + 1 \end{pmatrix}, \quad (30)$$

can be obtained by direct substitution of Eqs. (24), (25) and (26) into Eq. (27). Here \mathcal{N} is the norm of the vector λ . This factor becomes relevant only in the limiting cases $t_1 \rightarrow 0$ and $t_1 \rightarrow 1$ for Eqs. (29) and (30), respectively. In these cases, the vectors are given by

$$\lambda(0; 0) = - \begin{pmatrix} 0 \\ 0 \\ 1 \end{pmatrix}, \quad (31)$$

and

$$\lambda(1; 1) = \mathcal{N} \begin{pmatrix} \nu_2 \nu_3 (\nu_3 - \nu_2) \\ -\nu_3 (\nu_3 - 1) \\ \nu_2 (\nu_2 - 1) \end{pmatrix}, \quad (32)$$

respectively. These expressions are obtained by applying l'Hôpital's rule. The normalization factor \mathcal{N} in Eq. (32) differs from that in Eq. (30). In this context, it serves a purely technical purpose and is included for consistency with the examples later.

Using Eqs. (29) and (30) in the general inequality (14)

yields a set of tight inequalities,

$$-(\nu_3 - \nu_2)t_1^{\nu_3 + \nu_2 - 1}\mathcal{P}_1 + (\nu_3 - 1)t_1^{\nu_3}\mathcal{P}_2 - (\nu_2 - 1)t_1^{\nu_2}\mathcal{P}_3 \leq 0 \quad (33)$$

and

$$\begin{aligned} & (\nu_2 - \nu_3)t_1^{\nu_2 + \nu_3 - 1}(1 - \mathcal{P}_1) + (\nu_2 t_1^{\nu_2 - 1} - \nu_3 t_1^{\nu_3 - 1})\mathcal{P}_1 \\ & + (\nu_3 - 1)t_1^{\nu_3}(1 - \mathcal{P}_2) + (\nu_3 t_1^{\nu_3 - 1} - 1)\mathcal{P}_2 \\ & - (\nu_2 - 1)t_1^{\nu_2}(1 - \mathcal{P}_3) - (\nu_2 t_1^{\nu_2 - 1} - 1)\mathcal{P}_3 \leq 0. \end{aligned} \quad (34)$$

for $\tau = 0$ and $\tau = 1$, respectively. Equation (31) yields the trivial inequality $\mathcal{P}_3 \geq 0$. In contrast, Eq. (32) results in the nontrivial inequality,

$$\begin{aligned} & \nu_2\nu_3(\nu_3 - \nu_2)\mathcal{P}_1 - \nu_3(\nu_3 - 1)\mathcal{P}_2 + \nu_2(\nu_2 - 1)\mathcal{P}_3 \\ & \leq \nu_2\nu_3(\nu_3 - \nu_2) - \nu_3(\nu_3 - 1) + \nu_2(\nu_2 - 1), \end{aligned} \quad (35)$$

which provides a meaningful constraint on the classical set \mathcal{H} .

Linear inequalities (33) for all t_1 can be compactly combined into a single nonlinear inequality for the probabilities \mathcal{P}_i . This is achieved by maximizing the left-hand side of this inequality over the interval $t_1 \in [0, 1]$ and requiring that the maximum remains nonpositive. This procedure leads to the inequality

$$\mathcal{P}_2^{\nu_3 - 1} \leq \mathcal{P}_1^{\nu_3 - \nu_2}\mathcal{P}_3^{\nu_3 - \nu_2}. \quad (36)$$

For the inequalities (34), however, a similarly simple analytical reduction has not been identified.

It is useful to consider the special case with $\eta_1 = 1/3$, $\eta_2 = 2/3$, and $\eta_3 = 1$, which corresponds to $\nu_2 = 2$ and $\nu_3 = 3$. In this scenario, inequalities (33) and (34) can be interpreted as conditions for nonpositivity of quadratic trinomials of the variable t_1 . These inequalities hold whenever the corresponding trinomials have at least one real root or no real roots. This results in two nonlinear inequalities

$$\mathcal{P}_2^2 \leq \mathcal{P}_1\mathcal{P}_3 \quad (37)$$

and

$$[\mathcal{P}_1 - \mathcal{P}_2]^2 \leq [1 - \mathcal{P}_1][\mathcal{P}_2 - \mathcal{P}_3] \quad (38)$$

for $\tau = 0$ and $\tau = 1$, respectively. In this case, inequality (35) reduces to

$$3\mathcal{P}_1 - 3\mathcal{P}_2 + \mathcal{P}_3 \leq 1, \quad (39)$$

which is automatically satisfied whenever inequality (38) holds.

IV. HIGHER NUMBER OF SETTINGS

The technique described in the previous section can be generalized to an arbitrary number of settings, N . In this case, Eq. (8) takes the form

$$\Pi_i(t) = t^{\nu_i}, \quad (40)$$

where

$$\nu_i = \frac{\eta_i}{\eta_1}. \quad (41)$$

Here, $\nu_1 = 1$ and $1 < \nu_2 < \dots < \nu_N$. Of particular interest is the case where the discrete values η_i are uniformly distributed over the interval $[0, 1]$, i.e., $\eta_i = 1/N$. Nevertheless, we also consider a more general situation. A similar analysis was carried out in Ref. [49] for the photocounting distribution with an odd-dimensional vector \mathcal{P} . In the present scenario, it is likewise convenient to distinguish between odd and even N , although a fully general treatment is also possible but considerably more cumbersome.

Let us start with a consideration of the scenario with an odd number of settings, $N = 2m + 1$, where m is an integer. A direct generalization of Eq. (27) is given by

$$\boldsymbol{\lambda}(\mathbf{t}_m; \tau) = (-1)^{\tau+1}\mathcal{N}\left(\star \bigwedge_{k=1}^m \Delta\boldsymbol{\Pi}(t_k, \tau) \wedge \dot{\boldsymbol{\Pi}}(t_k)\right). \quad (42)$$

Here, $\Delta\boldsymbol{\Pi}(t_k, \tau)$ is defined in Eq. (28), $\tau = \pm 1$, and

$$\mathbf{t}_m = \{t_1, \dots, t_m\}, \quad 0 \leq t_1 \leq t_2 \leq \dots \leq t_m \leq 1. \quad (43)$$

The factor \mathcal{N} denotes normalization. The symbol \star represents the Hodge star, which generalizes the cross product; see Ref. [70] and Eq. (A1) in Appendix A. Applying this vector $\boldsymbol{\lambda}$, the left-hand side of inequality (14) reduces to

$$\begin{aligned} \boldsymbol{\lambda}(\mathbf{t}_m; \tau) \cdot \mathbf{P} &= \mathcal{N}(-1)^{\tau+1} \\ &\times \det \begin{pmatrix} \mathcal{P}_1 & \mathcal{P}_2 & \dots & \mathcal{P}_N \\ t_1 - \tau & t_1^{\nu_2} - \tau & \dots & t_1^{\nu_N} - \tau \\ 1 & \nu_2 t_1^{\nu_2 - 1} & \dots & \nu_N t_1^{\nu_N - 1} \\ \dots & \dots & \dots & \dots \\ t_m - \tau & t_m^{\nu_2} - \tau & \dots & t_m^{\nu_N} - \tau \\ 1 & \nu_2 t_m^{\nu_2 - 1} & \dots & \nu_N t_m^{\nu_N - 1} \end{pmatrix}. \end{aligned} \quad (44)$$

The function $\boldsymbol{\lambda}(\mathbf{t}_m; \tau) \cdot \boldsymbol{\Pi}(t)$ attains its global maximum at all points $t = t_i$ and $t = \tau$, see Fig. 4. Therefore, the right-hand side of inequality (14) takes the form

$$\begin{aligned} \sup_{t \in [0, 1]} \boldsymbol{\lambda}(\mathbf{t}_m; \tau) \cdot \boldsymbol{\Pi}(t) &= \mathcal{N}(-1)^{\tau+1} \\ &\times \det \begin{pmatrix} \tau & \tau & \dots & \tau \\ t_1 - \tau & t_1^{\nu_2} - \tau & \dots & t_1^{\nu_N} - \tau \\ 1 & \nu_2 t_1^{\nu_2 - 1} & \dots & \nu_N t_1^{\nu_N - 1} \\ \dots & \dots & \dots & \dots \\ t_m - \tau & t_m^{\nu_2} - \tau & \dots & t_m^{\nu_N} - \tau \\ 1 & \nu_2 t_m^{\nu_2 - 1} & \dots & \nu_N t_m^{\nu_N - 1} \end{pmatrix}. \end{aligned} \quad (45)$$

In the particular case $\eta_i = i/N$, the right-hand side simplifies to

$$\begin{aligned} \sup_{t \in [0, 1]} \boldsymbol{\lambda}(\mathbf{t}_m; \tau) \cdot \boldsymbol{\Pi}(t) &= \boldsymbol{\lambda}(\mathbf{t}_m; \tau) \cdot \boldsymbol{\Pi}(t_i) \\ &= \mathcal{N}\tau f(\mathbf{t}_m; 0)f(\mathbf{t}_m; 1)g(\mathbf{t}_m), \end{aligned} \quad (46)$$

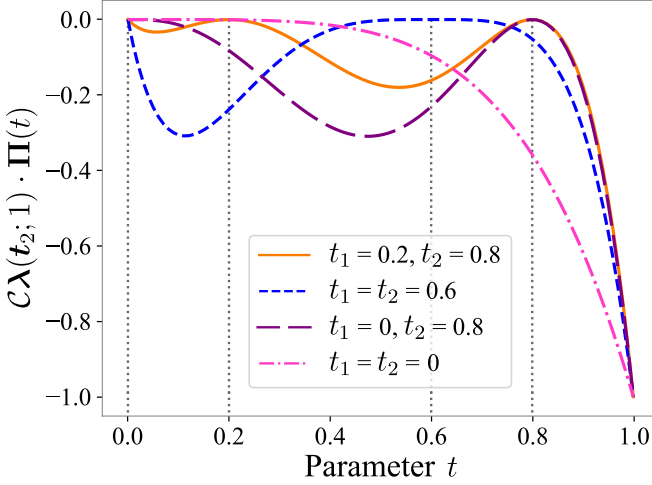


FIG. 4. The function $\lambda(\mathbf{t}_m; \tau) \cdot \Pi(t)$ for $\eta_i = i/N$, $N = 5$ (i.e., $m = 2$), and $\tau = 0$. The points $t = t_1$, $t = t_2$, and $t = \tau$ correspond to the global maximum. Depending on whether $t_1 = t_2$ or $t_2 = \tau$, the function exhibits $2^2 = 4$ different variants [see Eq. (50)], each with a different number of maxima. Here, $\mathcal{C} = \inf_{t \in [0,1]} \lambda(\mathbf{t}_m; \tau) \cdot \Pi(t)$ is a scaling factor introduced to make all plots comparable in scale.

where

$$f(\mathbf{t}_l; a) = \prod_{k=1}^l (t_k - a)^2, \quad (47)$$

$$g(\mathbf{t}_l) = \prod_{i < j}^l (t_i - t_j)^4. \quad (48)$$

For a detailed derivation and a proof that the corresponding inequalities form a complete set of tight inequalities, see Appendix B. An intuitive explanation of this form of λ is presented at the end of this section together with the case of even N .

Strictly speaking, the vector λ in the form of Eq. (42) can be directly applied only when $0 \leq t_1 < t_2 < \dots < t_m \leq 1$. Indeed, if $t_i = t_{i+1}$ for at least one index i , the determinant in this equation vanishes, while the normalization factor \mathcal{N} diverges. In such cases, the indeterminacy must be resolved using l'Hôpital's rule. The general expression for λ , which also covers the cases with coinciding t_i , is given by

$$\lambda(\mathbf{t}_m; \tau) = (-1)^{\tau+1} \mathcal{N} \times \star \left(\bigwedge_{k \in \mathcal{U}(\mathbf{t}_m)} \bigwedge_{j=\delta_{t_k, \tau}}^{2\omega(t_k)-1+\delta_{t_k, \tau}} \frac{\partial^j}{\partial t_k^j} \Delta \Pi(t_k, \tau) \right), \quad (49)$$

where $\mathcal{U}(\mathbf{t}_m)$ is the set of indices which correspond to unique elements of \mathbf{t}_m , $\omega(t_k)$ is the number of times t_k is included in \mathbf{t}_m . The normalization factor \mathcal{N} is defined separately for each such configuration.

The number of different configurations of $\lambda(\mathbf{t}_m; \tau)$ can be determined as follows. First, let $q = |\mathcal{U}(\mathbf{t}_m)|$ denote

the number of unique elements in \mathbf{t}_m . It can take values $q = 1, \dots, m$. Second, note that $\sum_{k \in \mathcal{U}(\mathbf{t}_m)} \omega(t_k) = m$. Third, for a fixed q , the set \mathbf{t}_m can be partitioned into q groups of equal elements t_i , with group sizes given by $\omega(t_k)$. The number of distinct partitions of \mathbf{t}_m into q groups is $\binom{m-1}{q-1}$. Moreover, for given q and $\omega(t_k)$, there exist two types of $\lambda(\mathbf{t}_m; \tau)$ depending on whether any component of \mathbf{t}_m equals τ . Thus, for a given τ , there are

$$\sum_{q=1}^m 2 \binom{m-1}{q-1} = 2^m \quad (50)$$

different variants of $\lambda(\mathbf{t}_m; \tau)$, each having q or $q+1$ global maximum points depending on whether any component of \mathbf{t}_m equals τ ; see Fig. 4.

Let us now consider the case of an even number of settings, $N = 2m$, with $m \geq 2$. In this case, geometrical arguments similar to those presented at the end of this section lead to two types of vectors λ ,

$$\lambda(\mathbf{t}_m) = \mathcal{N} \left(\star \bigwedge_{k=2}^m \Delta \Pi(t_k, t_1) \wedge \dot{\Pi}(t_k) \right) \wedge \dot{\Pi}(t_1) \quad (51)$$

and

$$\begin{aligned} \lambda(\mathbf{t}_{m-1}; 0, 1) = \\ - \mathcal{N} \left(\star \bigwedge_{k=1}^{m-1} \Delta \Pi(t_k, 0) \wedge \dot{\Pi}(t_k) \right) \wedge \Delta \Pi(1, 0), \end{aligned} \quad (52)$$

where \mathbf{t}_m is defined by Eq. (43). A proof that these vectors form a complete set of tight inequalities is given in Appendix B.

Firstly, we analyze in detail inequality (14) associated with λ given in Eq. (51). Its left-hand side is

$$\lambda(\mathbf{t}_m) \cdot \mathcal{P} = \mathcal{N} \det \begin{pmatrix} \mathcal{P}_1 & \mathcal{P}_2 & \dots & \mathcal{P}_N \\ t_2 - t_1 & t_2^{\nu_2} - t_1^{\nu_2} & \dots & t_2^{\nu_N} - t_1^{\nu_N} \\ 1 & \nu_2 t_2^{\nu_2-1} & \dots & \nu_N t_2^{\nu_N-1} \\ \dots & \dots & \dots & \dots \\ t_m - t_1 & t_m^{\nu_2} - t_1^{\nu_2} & \dots & t_m^{\nu_N} - t_1^{\nu_N} \\ 1 & \nu_2 t_m^{\nu_2-1} & \dots & \nu_N t_m^{\nu_N-1} \\ 1 & \nu_2 t_1^{\nu_2-1} & \dots & \nu_N t_1^{\nu_N-1} \end{pmatrix}. \quad (53)$$

Since the function $\lambda(\mathbf{t}_m) \cdot \Pi(t)$ attains its global maximum at all points $t = t_i$ (see Fig. 5a), the right-hand side is

$$\begin{aligned} \sup_{t \in [0,1]} \lambda(\mathbf{t}_m) \cdot \Pi(t) = \\ \mathcal{N} \det \begin{pmatrix} t_1 & t_1^{\nu_2} & \dots & t_1^{\nu_N} \\ t_2 - t_1 & t_2^{\nu_2} - t_1^{\nu_2} & \dots & t_2^{\nu_N} - t_1^{\nu_N} \\ 1 & \nu_2 t_2^{\nu_2-1} & \dots & \nu_N t_2^{\nu_N-1} \\ \dots & \dots & \dots & \dots \\ t_m - t_1 & t_m^{\nu_2} - t_1^{\nu_2} & \dots & t_m^{\nu_N} - t_1^{\nu_N} \\ 1 & \nu_2 t_m^{\nu_2-1} & \dots & \nu_N t_m^{\nu_N-1} \\ 1 & \nu_2 t_1^{\nu_2-1} & \dots & \nu_N t_1^{\nu_N-1} \end{pmatrix}. \end{aligned} \quad (54)$$

For the particular case $\eta_i = i/N$, the right-hand side simplifies to

$$\sup_{t \in [0,1]} \boldsymbol{\lambda}(\mathbf{t}_m) \cdot \boldsymbol{\Pi}(t) = \boldsymbol{\lambda}(\mathbf{t}_m; \tau) \cdot \boldsymbol{\Pi}(t_i) = f(\mathbf{t}_m; 0)g(\mathbf{t}_m), \quad (55)$$

where $f(\mathbf{t}_m; 0)$ and $g(\mathbf{t}_m)$ are defined in Eqs. (47) and (48), respectively.

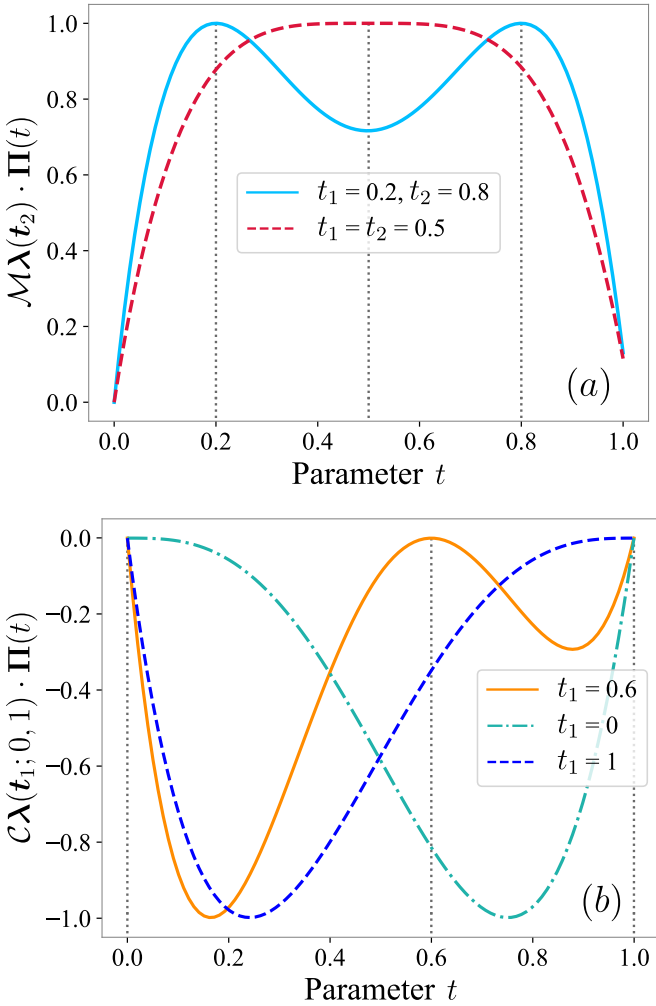


FIG. 5. The functions (a) $\boldsymbol{\lambda}(\mathbf{t}_m) \cdot \boldsymbol{\Pi}(t)$ and (b) $\boldsymbol{\lambda}(\mathbf{t}_{m-1}; 0, 1) \cdot \boldsymbol{\Pi}(t)$ are shown for $\eta_i = i/N$ with $N = 4$ (i.e., $m = 2$). For case (a), the points $t = t_1$ and $t = t_2$ correspond to the global maximum. For case (b), the points $t = 0$, $t = t_1$ and $t = 1$ correspond to the global maximum. Depending on whether $t_1 = t_2$, the function exhibits two distinct variants in case (a), and $2^3 - 1 = 7$ variants in case (b), where the cases $t_i = 0$ and $t_i = 1$ are also included. Here, $\mathcal{M} = \sup_{t \in [0,1]} \boldsymbol{\lambda}(\mathbf{t}_m) \cdot \boldsymbol{\Pi}(t)$ and $\mathcal{C} = \inf_{t \in [0,1]} \boldsymbol{\lambda}(\mathbf{t}_{m-1}; 0, 1) \cdot \boldsymbol{\Pi}(t)$ are scaling factors introduced to make all plots comparable in scale.

Similar to the case of odd N , Eq. (51) cannot be directly applied when $t_i = t_{i+1}$ for at least one value of i . Resolving this indeterminacy using l'Hôpital's rule leads

to the expression

$$\boldsymbol{\lambda}(\mathbf{t}_m) = \mathcal{N} \star \left(\bigwedge_{k \in \mathcal{U}(\mathbf{t}_m)} \bigwedge_{j=\delta_{t_k, t_1}}^{2\omega(t_k)-1} \frac{\partial^j}{\partial t_k^j} [\boldsymbol{\Pi}(t_k) - (1 - \delta_{t_k, t_1}) \boldsymbol{\Pi}(t_1)] \right), \quad (56)$$

where $\mathcal{U}(\mathbf{t}_m)$ and $\omega(t_k)$ are defined as after Eq. (49). The total number of distinct configurations is 2^{m-1} .

Secondly, we analyze in detail the inequality associated with $\boldsymbol{\lambda}(\mathbf{t}_{m-1}; 0, 1)$ given by Eq. (52). In this case, the left-hand side reads

$$\boldsymbol{\lambda}(\mathbf{t}_{m-1}; 0, 1) \cdot \mathcal{P} = -\mathcal{N} \det \begin{pmatrix} \mathcal{P}_1 & \mathcal{P}_2 & \dots & \mathcal{P}_N \\ t_1 & t_1^{\nu_2} & \dots & t_1^{\nu_N} \\ 1 & \nu_2 t_1^{\nu_2-1} & \dots & \nu_N t_1^{\nu_N-1} \\ \dots & \dots & \dots & \dots \\ t_{m-1} & t_{m-1}^{\nu_2} & \dots & t_{m-1}^{\nu_N} \\ 1 & \nu_2 t_{m-1}^{\nu_2-1} & \dots & \nu_N t_{m-1}^{\nu_N-1} \\ 1 & 1 & \dots & 1 \end{pmatrix}. \quad (57)$$

The global maximum of $\boldsymbol{\lambda}(\mathbf{t}_{m-1}; 0, 1) \cdot \boldsymbol{\Pi}(t)$ is attained at the points $t = t_i$ ($i = 1, \dots, m$), $t = 0$, and $t = 1$, and in each case the value is zero, see Fig. 5b. Thus, the right-hand side is given by

$$\sup_{t \in [0,1]} \boldsymbol{\lambda}(\mathbf{t}_{m-1}; 0, 1) \cdot \boldsymbol{\Pi}(t) = 0. \quad (58)$$

The general expression, which also covers the cases of equal t_i and t_{i+1} and requires resolving the indeterminacy using l'Hôpital's rule, is

$$\boldsymbol{\lambda}(\mathbf{t}_{m-1}; 0, 1) = \mathcal{N} \star \left(\Delta \boldsymbol{\Pi}(1, 0) \wedge \bigwedge_{k \in \mathcal{U}(\mathbf{t}_m)} \bigwedge_{j=\delta_{t_k, 0}+\delta_{t_k, 1}}^{2\omega(t_k)-1+\delta_{t_k, 0}+\delta_{t_k, 1}} \frac{\partial^j}{\partial t_k^j} \Delta \boldsymbol{\Pi}(t_k, \tau) \right), \quad (59)$$

The total number of distinct configurations is $2^{m+1} - 1$.

The vectors $\boldsymbol{\lambda}$ given by Eqs. (42), (51), and (52) form the set of tight inequalities defined by Eqs. (15) and (16). A detailed proof of this fact is provided in Appendix B. Despite the different explicit forms of $\boldsymbol{\lambda}$ for odd and even N , the underlying reasoning is structurally the same. To give an intuitive explanation, we first note that in both cases

$$\boldsymbol{\lambda} \cdot \dot{\boldsymbol{\Pi}}(t_i) = 0 \quad (60)$$

for $i = 1, \dots, m$. This implies that the vector $\boldsymbol{\lambda}$ is orthogonal to all vectors $\boldsymbol{\Pi}(t_i)$. Consequently, the points t_i satisfy the conditions for which the function $\dot{\boldsymbol{\Pi}}(t) \cdot \boldsymbol{\lambda}$ reaches its extrema, as required by Eq. (15). Next, we observe that

$$\boldsymbol{\lambda} \cdot \Delta \boldsymbol{\Pi}(t_i, t_k) = 0, \quad (61)$$

where we additionally set $t_{0,m+1} = \tau \in 0, 1$ for odd N . Thus, the vector λ is also orthogonal to the vectors $\Delta\mathbf{\Pi}(t_i, t_k)$. Using Eq. (28), we conclude that $\lambda \cdot \mathbf{\Pi}(t)$ takes the same value for all $t = t_i$, including $k = 0, m+1$ in the odd- N case. Combining this observation with the considerations of Ref. [49] (see also Appendix B), we conclude that these points are indeed global maxima of the functions $\lambda \cdot \mathbf{\Pi}(t)$. Their values are given explicitly by Eqs. (45) and (55). Examples of such functions are shown in Figs. 4 and 5.

V. NONLINEAR INEQUALITIES WITH UNIFORMLY DISTRIBUTED EFFICIENCIES

In this section, we focus on the special case of uniformly distributed efficiencies, i.e., $\eta_i = i/N$. In this setting, Eq. (13) can be rewritten as

$$\mathcal{P}_i = \int_0^1 dt \varrho(t) t^i. \quad (62)$$

This implies that the no-click probabilities $\mathcal{P}_i = \mathcal{P}(0|\eta_i)$ can be simulated with classical radiation if and only if they can be treated as the moments of a probability distribution $\varrho(t)$ with $t \in [0, 1]$. Here we consider $i = 0, \dots, N$, which ensures that $\mathcal{P}_0 = \mathcal{P}(0|\eta_0) = 1$.

Now we can apply a necessary and sufficient condition for the existence of a distribution $\varrho(t)$ whose statistical moments are given by the values \mathcal{P}_i , namely the Hausdorff moment problem. According to Ref. [68], this condition holds if and only if two quadratic forms, indexed by $k = 1, 2$,

$$F^{(k)}(\mathbf{x}) = \sum_{i,j=0}^{m_{\max}} M_{i,j}^{(k)} x_i x_j, \quad (63)$$

are non-negative. Here, $\mathbf{x} = \{x_1, \dots, x_N\}$ with $x_i \in \mathbb{R}$, and $M_{i,j}^{(k)}$ together with m_{\max} are defined as

$$M_{i,j}^{(1)} = \mathcal{P}_{i+j}, \quad m_{\max} = m, \quad (64)$$

$$M_{i,j}^{(2)} = \mathcal{P}_{i+j} - \mathcal{P}_{i+j+2}, \quad m_{\max} = m - 1. \quad (65)$$

for $N = 2m$ and

$$M_{i,j}^{(1)} = \mathcal{P}_{i+j+1}, \quad m_{\max} = m, \quad (66)$$

$$M_{i,j}^{(2)} = \mathcal{P}_{i+j} - \mathcal{P}_{i+j+1}, \quad m_{\max} = m. \quad (67)$$

for $N = 2m + 1$. Since $F^{(k)}(\mathbf{x})$ is linear with respect to \mathcal{P}_i , the inequalities $F^{(k)}(\mathbf{x}) \geq 0$ can be considered as a special case of inequality (14), with λ parameterized by $\mathbf{x} \in \mathbb{R}^N$ and the right-hand side equal to zero.

According to Sylvester's criterion, the quadratic form (63) is non-negative if and only if all its principal minors are non-negative. This allows us, for a given N , to formulate a set of nonlinear inequalities associated with minors of different orders. Applying these inequalities

requires significantly fewer computational resources compared with the optimization over \mathbf{t}_m and \mathbf{t}_{m-1} needed for the inequalities discussed in Sec. IV. The drawback of this approach is that it applies only to the case $\eta_i = i/N$.

Let us consider two simple examples. For $N = 2$ and $N = 4$, only the second-order minors are involved. They are given by

$$\det \begin{pmatrix} M_{0,0}^{(k)} & M_{0,1}^{(k)} \\ M_{1,0}^{(k)} & M_{1,1}^{(k)} \end{pmatrix} = M_{0,0}^{(k)} M_{1,1}^{(k)} - M_{1,0}^{(k)2} \geq 0. \quad (68)$$

In the case of two settings, $N = 2$, we obtain two inequalities: inequality (22) for $\nu_2 = 2$ and the trivial inequality $\mathcal{P}_2 \leq 1$, corresponding to $k = 1$ and $k = 2$, respectively. Inequality (23) represents a trivial statement. For three settings ($N = 3$), we again obtain two inequalities: (37) and (38), corresponding to $k = 1$ and $k = 2$, respectively.

More involved examples with $N = 4$ and $N = 5$ lead to the inequalities

$$\begin{pmatrix} M_{0,0}^{(k)} & M_{0,1}^{(k)} & M_{0,2}^{(k)} \\ M_{1,0}^{(k)} & M_{1,1}^{(k)} & M_{1,2}^{(k)} \\ M_{2,0}^{(k)} & M_{2,1}^{(k)} & M_{2,2}^{(k)} \end{pmatrix} \geq 0. \quad (69)$$

This condition implies the non-negativity of all principal minors of the 3×3 matrix. Equivalently, one may require that all three eigenvalues of the matrix are non-negative, for each k .

VI. AN EXAMPLE: PHASE-SQUEEZED COHERENT STATES

In this section, we present an example that demonstrates the applicability of our method. Before addressing a specific state, we briefly outline the methodology for practical applications of the derived inequalities. The simplest scenario corresponds to uniformly distributed efficiencies, $\eta_i = i/N$, considered in Sec. V. In this case, it is sufficient to verify the positive semidefiniteness of the matrices $M_{i,j}^{(k)}$ for $k = 1, 2$, either by applying Sylvester's criterion or by checking the non-negativity of their eigenvalues.

In the general case of arbitrary $\eta = \{\eta_1, \dots, \eta_N\}$, we need to determine the maximal violation of inequality (14), which is given by

$$V(\eta) = \max_{\mathbf{t}_l, T} [\lambda(\mathbf{t}_l; T) \cdot \mathcal{P} - \lambda(\mathbf{t}_l; T) \cdot \mathbf{\Pi}(t_i)]. \quad (70)$$

Here, $l = m$ or $l = m - 1$, and T can take the values $\tau = 0, \tau = 1, \emptyset$, or $0, 1$, depending on which vector λ is used. To compute this maximum, we first consider the vectors λ given by Eq. (42) for odd N , and by Eqs. (51) and (52) for even N . If the optimization yields a vector \mathbf{t}_l such that $t_{i+1} - t_i < \varepsilon$ for at least one index i (with ε being a fixed small value), we then proceed with the generalized vectors: Eq. (49) for odd N , and Eqs. (56) and (59) for even N .

In practical scenarios, it is reasonable to consider the case of uniformly distributed efficiencies, $\eta_i = i/N$. However, these efficiencies are typically known only with some uncertainty, represented by the error vector $\boldsymbol{\delta} = \{\delta_1, \dots, \delta_N\}$, such that $\eta_i = i/N + \delta_i$. We assume that $\boldsymbol{\delta}$ lies within a domain Δ . To certify nonclassicality in this setting, one must verify that, for the given vector \mathcal{P} , the maximal violation $V(\boldsymbol{\eta})$ remains positive throughout the entire domain Δ . This means that if

$$\min_{\boldsymbol{\delta} \in \Delta} V(\boldsymbol{\eta}_0 + \boldsymbol{\delta}) \leq 0, \quad (71)$$

where $\boldsymbol{\eta}_0 = \{1/N, 2/N, \dots, 1\}$, then there exists some $\boldsymbol{\delta} \in \Delta$ for which the vector \mathcal{P} can be reproduced by a statistical mixture of coherent states. Therefore, the certification of nonclassicality requires a strict violation of this inequality.

We illustrate our method using the phase-squeezed coherent state $|r, \alpha_0\rangle = \hat{D}(\alpha_0)\hat{S}(r)|0\rangle$, where $\hat{D}(\alpha_0)$ is the displacement operator, $\hat{S}(r)$ is the squeezing operator, and $|0\rangle$ is the vacuum state. Throughout, we assume that the coherent amplitude $\alpha_0 \in \mathbb{R}$ and the squeezing parameter $r > 0$. Phase-insensitive measurements, such as photocounting, are usually regarded as unsuitable for revealing nonclassicality of this state [6]. However, Ref. [49] demonstrated that such a test remains possible even with imperfect photon-number resolution, as encountered in arrays of on-off detectors. Here we further show that nonclassicality certification of these states is achievable even with a single on-off detector, by using the detection efficiency as a device setting.

The no-click probability for the squeezed coherent state $|r, \alpha_0\rangle$ is given by

$$\mathcal{P}(0|\eta) = \frac{1}{\sqrt{1 + \eta(2 - \eta) \sinh^2 r}} \times \exp \left[(\alpha_0^* - \alpha_0) \boldsymbol{\sigma}^{-1} \begin{pmatrix} -\alpha_0 \\ \alpha_0^* \end{pmatrix} \right], \quad (72)$$

where

$$\boldsymbol{\sigma}^{-1} = \frac{\eta}{4 [1 + \eta(2 - \eta) \sinh^2 r]} \times \begin{pmatrix} \eta \cosh 2r + 2 - \eta & -\eta \sinh 2r \\ -\eta \sinh 2r & \eta \cosh 2r + 2 - \eta \end{pmatrix}. \quad (73)$$

We construct the vector \mathcal{P} from the components $\mathcal{P}_i = \mathcal{P}(0|\eta_i)$, where η_i denotes the detection efficiency. These results are then used in the derived inequalities to test nonclassicality.

Let us consider the case $N = 3$. We begin with the simplest scenario of uniformly distributed efficiencies, $\eta_i = i/3$. As discussed in Sec. V, the corresponding nonlinear inequalities (37) and (38) apply in this case. The violations of these inequalities are quantified by

$$V = \max \left\{ \mathcal{P}_2^2 - \mathcal{P}_1 \mathcal{P}_3; (\mathcal{P}_1 - \mathcal{P}_2)^2 - (1 - \mathcal{P}_1)(\mathcal{P}_2 - \mathcal{P}_3) \right\}. \quad (74)$$

The dependence of V on the coherent amplitude α_0 is shown in Fig. 6. A clear violation is observed for small values of α_0 , which gradually disappears as α_0 increases. However, the magnitude of the violation is relatively small, making an accurate estimation of statistical errors essential in this regime. This can be addressed straightforwardly by employing the inequalities in the linear form Eq. (14).

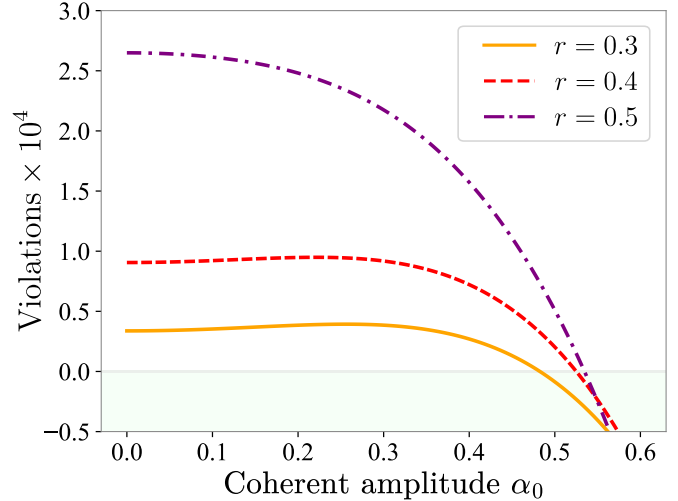


FIG. 6. Violation of the nonlinear inequalities (37) and (38) [see Eq. (74)] as a function of the coherent amplitude α_0 for phase-squeezed coherent states with different squeezing parameters r . The number of settings is $N = 3$, and the detection efficiency is $\eta_c = 0.8$. The shaded region corresponds to $V \leq 0$, for which no nonclassicality is detected.

Next, we consider a scenario in which the detection efficiencies are known only within a finite uncertainty. In this case, witnessing nonclassicality requires a violation of inequality (71), meaning that the quantity

$$V = \min_{\boldsymbol{\delta} \in \Delta} V(\boldsymbol{\eta}_0 + \boldsymbol{\delta}) \quad (75)$$

must be non-negative. To assess the statistical significance of such a violation, we estimate the uncertainty associated with the left-hand side of the underlying linear inequality, $\boldsymbol{\lambda}(t_l; T) \cdot \mathcal{P}$. Since this expression represents a sum of expectation values of the random variables corresponding to the components λ_i , its statistical error can be evaluated as

$$\epsilon = \sqrt{\frac{1}{M} \sum_{i=1}^N \text{Var}(\lambda_i)}, \quad (76)$$

where M is the total number of experimental trials. Here, each λ_i is treated as a random variable that takes the value λ_i when a no-click event occurs at the corresponding efficiency setting and 0 otherwise. During the optimization over the setting inaccuracies $\boldsymbol{\delta} \in \Delta$, we select the error configuration at which the minimum in Eq. (75) is attained. The resulting behavior is shown in Fig. 7.

One observes that a statistically significant violation can be achieved with a sample size of $M = 10^7$.

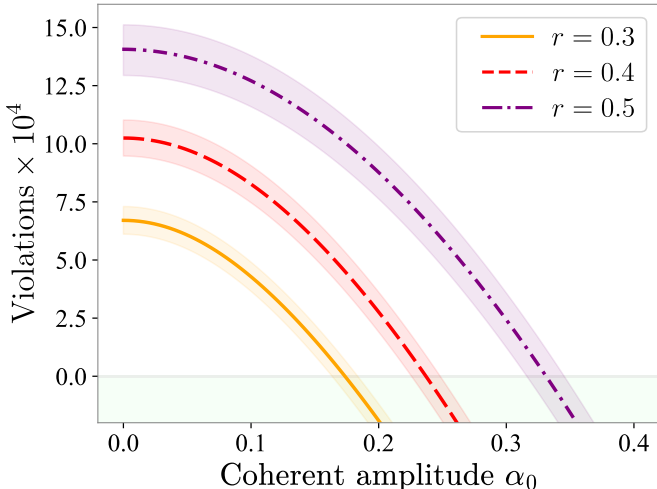


FIG. 7. Violation of inequality (71) [see Eq. (75)] as a function of the coherent amplitude α_0 for phase-squeezed coherent states with different squeezing parameters r . The remaining parameters are the same as in Fig. 6. The optimization is performed over the domain defined by $|\delta_i| \leq 0.01$ for all $i = 1, \dots, N$. The confidence intervals correspond to $M = 10^7$ measurement trials.

VII. SUMMARY AND CONCLUSION

In this paper, we have shown that, although a single on-off detector is generally regarded as unsuitable for detecting optical nonclassicality of quantum states, it can nevertheless be employed for this purpose after a simple modification. Specifically, we propose to precede the detector with a tunable attenuator that introduces controlled additional losses into the signal. A discrete set of N attenuation values then defines a corresponding set of effective detection efficiencies, which can be interpreted as distinct detector settings. In an experiment, one measures the no-click probabilities associated with each setting; collectively, these probabilities form a vector \mathcal{P} in an abstract N -dimensional Euclidean space.

The set of all vectors \mathcal{P} that can be reproduced by classical states, i.e., by statistical mixtures of coherent states, forms a convex set—the convex hull of the curve defined by the no-click probabilities of coherent states. Because the measurement scheme considered here is not tomographically complete, vectors generated by nonclassical states may still lie within this set, implying that nonclassicality cannot always be revealed by this measurement alone. However, if a given vector \mathcal{P} lies outside this convex set, the corresponding quantum state necessarily exhibits optical nonclassicality.

To determine whether a given vector \mathcal{P} belongs to the convex hull of classical vectors, we employ tools from convex geometry, in particular the hyperplane separation

theorem. This approach naturally leads to a continuous family of inequalities that are linear in the components of \mathcal{P} . Together, these inequalities provide a necessary and sufficient condition for membership of \mathcal{P} in the classical set. Violation of any of these inequalities certifies the nonclassicality of the corresponding quantum state.

If uniformly distributed efficiency settings are chosen, the problem is considerably simplified. In this case, the continuous family of linear inequalities can be replaced by a discrete set of nonlinear inequalities. This approach is computationally efficient and straightforward to implement. However, it is not robust against uncertainties in the efficiency values, which makes its direct application in realistic experimental scenarios challenging.

The method based on linear inequalities, however, can be naturally extended to scenarios in which the detection efficiencies are known only within finite uncertainties. Since these inequalities are formulated for arbitrary detector settings, one can introduce an additional optimization to test whether the measured vector \mathcal{P} can be compatible with a classical description for at least one configuration of efficiencies within a predetermined uncertainty region. If no such configuration exists, one can conclude that the proposed method reveals optical nonclassicality even under imperfect knowledge of experimental parameters, making it particularly relevant for practical implementations.

We have demonstrated that our technique, while being straightforward to implement experimentally, can reveal nonclassicality in scenarios where standard methods fail. As an illustrative example, we considered phase-squeezed coherent states. These states constitute an emblematic case: despite being nonclassical, they exhibit super-Poissonian photocounting statistics and are therefore often regarded as unsuitable for nonclassicality tests based on phase-insensitive measurements. Nevertheless, our approach overcomes this limitation and successfully reveals nonclassicality using only three efficiency settings. This example highlights the strong potential of our method for experimental applications and demonstrates its usefulness in situations where conventional techniques are ineffective.

ACKNOWLEDGMENT

The authors thank B. Hage and F. Hübner for enlightening discussions. V.S.K. acknowledges support from the National Research Foundation of Ukraine under Project No. 2023.03/0165. A.A.S. acknowledges support from the National Academy of Sciences of Ukraine through Project No. 0125U000031, from Simons Foundation International SFI-PD-Ukraine-00014573, PI LB, and from the Virtual Ukraine Institute for Advanced Study (VUIAS) as a 2025/2026 Fellow.

Appendix A: Hodge star

In this section, we recall the definition of the Hodge star operator used in Sec. IV for constructing the vectors λ . Consider the Euclidean space \mathbb{R}^n and a set of $(n-1)$ vectors \mathbf{v}^i , with $i = 1, \dots, n-1$. The Hodge star maps their exterior product to a vector in \mathbb{R}^n according to

$$\star \bigwedge_{i=1}^{n-1} \mathbf{v}^i = \begin{vmatrix} \mathbf{e}^1 & \mathbf{e}^2 & \dots & \mathbf{e}^n \\ v_1^1 & v_2^1 & \dots & v_n^1 \\ \vdots & \vdots & \ddots & \vdots \\ v_1^{n-1} & v_2^{n-1} & \dots & v_n^{n-1} \end{vmatrix}, \quad (\text{A1})$$

where $\mathbf{e}^1, \mathbf{e}^2, \dots, \mathbf{e}^n$ denotes an orthonormal basis of \mathbb{R}^n . This construction generalizes the cross product in \mathbb{R}^3 to arbitrary dimension n .

Appendix B: Tightness of inequalities

In this section, we prove that the inequalities associated with the vectors λ introduced in Sec. IV form a complete set of tight inequalities. To this end, we employ methods from convex geometry. In particular, our analysis relies on results from the theory of generalized moment problems and extended Chebyshev systems. The mathematical results used throughout this section can be found in Ref. [68]. We start with presenting general statements that apply to a broad class of measurements and experimental settings. In particular, these results cover both the photocounting statistics studied in Ref. [49] and the no-click statistics obtained from on-off detectors with tunable efficiency settings considered here. The explicit application of these general results to the latter case is discussed at the end of this section.

Let us consider a set of $N+1$ functions $\{\Pi_0^*(t), \dots, \Pi_N^*(t)\}$ that are N times differentiable on the interval $t \in [a, b]$. This set is called an extended Chebyshev system if there exists $\sigma = \pm 1$ such that

$$\sigma \Delta(t_0, \dots, t_N) > 0 \text{ if } a \leq t_0 \leq \dots \leq t_N \leq b, \quad (\text{B1})$$

where

$$\Delta(t_1, \dots, t_N) = \det \left(\Pi_0^{*(\omega_0)}(t_0) \ \dots \ \Pi_N^{*(\omega_N)}(t_N) \right). \quad (\text{B2})$$

Here

$$\Pi^{*(\omega_i)}(t_i) = \left(\Pi_1^{*(\omega_i)}(t_i) \ \Pi_2^{*(\omega_i)}(t_i) \ \dots \ \Pi_N^{*(\omega_i)}(t_i) \right)^T, \quad (\text{B3})$$

$i = 0, \dots, N$, and the superscript (ω_i) denotes the ω_i th derivative. The integer ω_i equals the number of occurrences of t_i in the sequence t_0, \dots, t_{i-1} , with the convention $\omega_0 = 0$. In this context, a linear combination of functions from an extended Chebyshev system

$$P(t) = \sum_{i=0}^N \lambda_i^* \Pi_i^*(t) = \lambda^* \cdot \Pi^*(t) \quad (\text{B4})$$

is called a generalized polynomial. An equivalent defining property of an extended Chebyshev system is that any generalized polynomial has at most N zeros on $[a, b]$, counted with multiplicities.

Our task is to determine the conditions under which a vector $\mathcal{P}^* \in \mathbb{R}^{N+1}$ belongs to the convex set generated by the vectors $\Pi^*(t)$. In this context, a crucial role is played by vectors λ^* that correspond to generalized polynomials non-negative on the interval $t \in [a, b]$, i.e., $P(t) \geq 0$. The following theorem makes this connection precise.

Theorem 1. *A vector $\mathcal{P}^* \in \mathbb{R}^{N+1}$ can be represented as a convex combination of the vectors $\Pi^*(t)$, $t \in [a, b]$, iff for any non-negative generalized polynomial $P(t) = \lambda^* \cdot \Pi^*(t) \geq 0$, the dot product*

$$\lambda^* \cdot \mathcal{P}^* \geq 0. \quad (\text{B5})$$

The set of all vectors λ^* associated with non-negative generalized polynomials can be reduced without loss of generality to those corresponding to polynomials with exactly N zeros, counting multiplicities, in the interval $t \in [a, b]$. We refer to such polynomials as tight polynomials. The following theorem provides a key result that justifies this reduction and enables an optimization of the admissible set of λ^* .

Theorem 2 (Karlin). *Any non-negative generalized polynomial which is not tight can be uniquely decomposed into the sum of two tight generalized polynomials.*

Indeed, let us suppose that $\lambda_k^* \cdot \mathcal{P}^* \geq 0$ holds for every λ_k^* associated with a tight generalized polynomial. By Karlin's Theorem, any non-negative generalized polynomial $P(t) = \lambda^* \cdot \Pi^*(t)$ can be decomposed into the sum of two tight generalized polynomials, $P_1(t)$ and $P_2(t)$. This decomposition induces a corresponding decomposition of the coefficient vector, $\lambda^* = \lambda_1^* + \lambda_2^*$, where each vector λ_k^* is associated with a tight polynomial. Consequently,

$$\lambda^* \cdot \mathcal{P}^* = (\lambda_1^* + \lambda_2^*) \cdot \mathcal{P}^* = \lambda_1^* \cdot \mathcal{P}^* + \lambda_2^* \cdot \mathcal{P}^*. \quad (\text{B6})$$

Since both terms on the right-hand side are non-negative by assumption, it follows that $\lambda^* \cdot \mathcal{P}^* \geq 0$. Therefore, it is sufficient to test the inequalities associated with tight generalized polynomials in order to determine whether \mathcal{P}^* belongs to the convex hull.

Let us now consider a specific measurement scheme, described by POVM elements associated with the set $\{\Pi_i(t) | i = 1, \dots, N\}$. We define the extended set of functions by $\Pi_0^*(t) = 1$ and $\Pi_i^*(t) = \Pi_i(t)$ for $i = 1, \dots, N$, and assume that this set forms an extended Chebyshev system on $[a, b]$. Our goal is to determine whether a given vector \mathcal{P} can be presented as a convex combination of the vectors $\Pi(t)$. To this end we introduce the extended vector \mathcal{P}^* with components $\mathcal{P}_0^* = 1$ and $\mathcal{P}_i^* = \mathcal{P}_i$ for $i = 1, \dots, N$. It is straightforward to see that the vector \mathcal{P} is a convex combination of $\Pi(t)$ iff the vector \mathcal{P}^* is a convex combination of $\Pi^*(t)$.

In the the present setting, a generalized polynomial $\boldsymbol{\lambda}^* \cdot \boldsymbol{\Pi}^*(t)$ is non-negative, if it satisfies the inequality

$$\lambda_0^* \geq \boldsymbol{\lambda} \cdot \boldsymbol{\Pi}(t). \quad (\text{B7})$$

Here we have assumed that

$$\boldsymbol{\lambda}^* = \begin{pmatrix} \lambda_0 \\ -\boldsymbol{\lambda} \end{pmatrix}. \quad (\text{B8})$$

Additionally, inequality (B5) can be equivalently rewritten as

$$\lambda_0^* \geq \boldsymbol{\lambda} \cdot \boldsymbol{\mathcal{P}}. \quad (\text{B9})$$

Consider a family of non-negative generalized polynomials that share a fixed $\boldsymbol{\lambda}$ but have different λ_0^* . Each polynomial produces inequality (B9) with its own λ_0^* . Since inequality (B9) gives an upper bound on $\boldsymbol{\lambda} \cdot \boldsymbol{\mathcal{P}}$, the inequality with the smallest admissible λ_0^* , as all others are implied by it. According to Eq. (B7), this minimal value is

$$\lambda_0^* = \sup_{t \in [a,b]} \boldsymbol{\lambda} \cdot \boldsymbol{\Pi}(t). \quad (\text{B10})$$

Thus, we conclude that in order to verify if $\boldsymbol{\mathcal{P}}^*$ belongs to the convex hull of the vectors $\boldsymbol{\Pi}^*(t)$ one only needs to consider generalized polynomials satisfying Eq. (B10). Substituting it into inequality (B9) directly yields inequality (14).

Now we show that tight generalized polynomials correspond to the set Λ of tight inequalities; see Sec. II. First, by virtue of Theorem 2, any vector $\boldsymbol{\lambda}^*$ can be decomposed into a sum of two vectors $\boldsymbol{\lambda}_k^*$ associated with tight generalized polynomials. It then follows directly that any vector $\boldsymbol{\lambda}$ defining inequalities of the form (14) can likewise be decomposed into a sum of corresponding vectors $\boldsymbol{\lambda}_k$. Second, we need to prove that a given vector $\boldsymbol{\lambda}_k$ cannot be expressed as a linear combination of other vectors from this set. For this purpose, we outline a useful representation of a generalized polynomial with N zeros t_1, \dots, t_N , where the number of duplications of a zero indicates its multiplicity. Such a polynomial is determined uniquely up to a constant factor C and is given by

$$C\Delta(t, t_1, \dots, t_N), \quad (\text{B11})$$

cf. Eq. (B2). It implies that a tight generalized polynomial cannot be decomposed into the sum of other linearly independent generalized polynomials. Indeed, if that were the case, they would need to have the same zeros and multiplicities as the original tight generalized polynomial. But that contradicts the uniqueness property. This conclusion translates directly to the corresponding inequalities of the form (14).

As the next step, we derive explicit expressions for the tight test functions. According to Eq. (B11), a tight generalized polynomial is determined by its zeros up to a constant factor C . Since such a polynomial is non-negative on the interval, all its interior zeros must be non-nodal, i.e., their multiplicities must be even. We denote a tight generalized polynomial by $P(t; \mathbf{t}_l; T)$, where $\mathbf{t}_l = \{t_1, \dots, t_l\}$ is a set of interior zeros of size $l = (N - |T|)/2$ such that every occurrence of a zero increases its multiplicity by 2, e.g., $\{0.2, 0.2, 0.9\}$ means that 0.2 has a multiplicity of 4 and 0.9 has a multiplicity of 2. The symbol T denotes the set of boundary zeros such that there are no duplications and each occurrence of a zero increases its multiplicity by 1 and $|T|$ denotes the cardinality of this set (the number of elements). Depending on the specific vector $\boldsymbol{\lambda}(\mathbf{t}_l; T)$, under consideration, the set T may contain the boundary points a, b , or be empty.

For each parity of N , there are two families of tight generalized polynomials. If $N = 2m$, for the first family, $T = \emptyset$ and $\mathbf{t}_m = \{t_1, \dots, t_m\}$,

$$P(t; \mathbf{t}_m) = \sigma C \Delta(t, t_1, t_1, \dots, t_m, t_m), \quad (\text{B12})$$

where $C > 0$ and σ from Eq. (B1) ensures that the polynomial is non-negative. For the second family, $T = \{a, b\}$ and $\mathbf{t}_{m-1} = \{t_1, \dots, t_{m-1}\}$,

$$\begin{aligned} P(t; \mathbf{t}_{m-1}; a, b) \\ = -\sigma C \Delta(t, a, t_1, t_1, \dots, t_{m-1}, t_{m-1}, b), \end{aligned} \quad (\text{B13})$$

where $C > 0$ and the minus sign accounts for the swap of t and a . If $N = 2m + 1$, we have $\mathbf{t}_m = \{t_1, \dots, t_m\}$ for both families and $T = \{a\}$ and $T = \{b\}$ for the first and the second family, respectively,

$$P(t; \mathbf{t}_m; \tau) = (-1)^{\tau+1} \sigma C \Delta(t, \tau, t_1, t_1, \dots, t_m, t_m), \quad (\text{B14})$$

where $\tau = a, b$, $C > 0$.

We now derive the explicit expression for the vectors $\boldsymbol{\lambda}$ associated with tight inequalities. For clarity, we restrict the derivation to the case in which the set \mathbf{t}_m contains no duplications ($\omega_i = 1$) as the methodology remains the same for the general case. We substitute Eq. (B2) into Eq. (B12) and perform elementary column operations—namely, subtracting the second column from the first and applying the same operation to all columns with even indices in the determinant. As a result, the first row acquires a single nonzero entry, which allows us to expand the determinant along this row. This reduces the determinant to an $N \times N$ form,

$$P(t; \mathbf{t}_m) = \sigma C \det = -\sigma C \det \begin{pmatrix} \Delta\Pi_1(t, t_1) & \dot{\Pi}_1(t_1) & \dots & \Delta\Pi_1(t_m, t_1) & \dot{\Pi}_1(t_m) \\ \vdots & \vdots & \ddots & \vdots & \vdots \\ \Delta\Pi_N(t, t_1) & \dot{\Pi}_N(t_1) & \dots & \Delta\Pi_N(t_m, t_1) & \dot{\Pi}_N(t_m) \end{pmatrix}. \quad (\text{B15})$$

This expression can be further rearranged as

$$P(t; \mathbf{t}_m) = -\sigma C \left[-\det \left(\mathbf{\Pi}(t_1) \ \dot{\Pi}(t_1) \ \dots \ \Delta\mathbf{\Pi}(t_m, t_1) \ \dot{\Pi}(t_m) \right) + \det \left(\mathbf{\Pi}(t) \ \dot{\Pi}(t_1) \ \dots, \Delta\mathbf{\Pi}(t_m, t_1) \ \dot{\Pi}(t_m) \right) \right], \quad (\text{B16})$$

where we use vector notation for the matrix columns.

Since $P(t; \mathbf{t}_m) = \sup_{t' \in [a, b]} \boldsymbol{\lambda}(\mathbf{t}_m) \cdot \mathbf{\Pi}(t') - \boldsymbol{\lambda}(\mathbf{t}_m) \cdot \mathbf{\Pi}(t)$, where $\boldsymbol{\lambda}(\mathbf{t})$ is the associated tight test function, we conclude that

$$\begin{aligned} & \boldsymbol{\lambda}(\mathbf{t}_m) \cdot \mathbf{\Pi}(t) \\ &= \sigma C \det \left(\mathbf{\Pi}(t) \ \dot{\Pi}(t_1) \ \dots \ \Delta\mathbf{\Pi}(t_m, t_1) \ \dot{\Pi}(t_m) \right) \end{aligned} \quad (\text{B17})$$

Recall that the determinant of a matrix formed by a vector \mathbf{v} and a set of vectors $\mathbf{u}_1, \dots, \mathbf{u}_N$ can be written as the dot product

$$\det(\mathbf{v} \ \mathbf{u}_1 \ \dots \ \mathbf{u}_N) = \mathbf{v} \cdot \star(\mathbf{u}_1 \wedge \dots \wedge \mathbf{u}_N). \quad (\text{B18})$$

Then Eq. (B19) can be rewritten as

$$\begin{aligned} & \boldsymbol{\lambda}(\mathbf{t}) \cdot \mathbf{\Pi}(t) \\ &= \sigma C \mathbf{\Pi}(t) \cdot \star \left(\dot{\Pi}(t_1) \wedge \bigwedge_{i=2}^m \Delta\mathbf{\Pi}(t_i, t_1) \wedge \dot{\Pi}(t_i) \right). \end{aligned} \quad (\text{B19})$$

Thus,

$$\boldsymbol{\lambda}(\mathbf{t}) = \sigma \mathcal{N} \star \left(\dot{\Pi}(t_1) \wedge \bigwedge_{i=2}^m \Delta\mathbf{\Pi}(t_i, t_1) \wedge \dot{\Pi}(t_i) \right), \quad (\text{B20})$$

where we set $C = \mathcal{N}$. Similarly, one can obtain the expressions for other test functions.

As the next step, we specify the elements $\Pi_i(t)$ as those corresponding to the no-click statistics given by Eq. (40). According to Ref. [67],

$$\{1, t, t^{\nu_2}, \dots, t^{\nu_N}\}, \quad (\text{B21})$$

where $1 < \nu_2 < \dots < \nu_N$, is an extended Chebyshev system on $[0, 1]$. To address the singularity at the boundary point $t = 0$, we employ a limiting argument. We first derive the family of tight inequalities on the truncated interval $[\epsilon, 1]$ for an arbitrary $\epsilon \in]0, 1[$. Observe that for any $\epsilon_1 < \epsilon_2$, the inequalities associated with ϵ_2 follow directly from those associated with ϵ_1 . Consequently, the limiting inequalities derived as $\epsilon \rightarrow +0$ are sufficient to imply the inequalities for all $\epsilon \in]0, 1[$.

Now, let us determine the sign $\sigma = \pm 1$ from Eq. (B1). Since σ is the same across all the domain of t_0, \dots, t_N , we may restrict our attention to the case when there are no duplicates. As stated in Ref. [67],

$$\det \begin{pmatrix} \exp(x_0 y_0) & \exp(x_0 y_1) & \dots & \exp(x_0 y_N) \\ \exp(x_1 y_0) & \exp(x_1 y_1) & \dots & \exp(x_1 y_N) \\ \vdots & \vdots & \ddots & \vdots \\ \exp(x_N y_0) & \exp(x_N y_1) & \dots & \exp(x_N y_N) \end{pmatrix} > 0, \quad (\text{B22})$$

where $x_0 < \dots < x_N$ and $y_0 < \dots < y_N$. Substituting $x_0 = 0$, $x_i = \nu_i$, $i = 1, \dots, N$, and $y_j = \ln t_j$, $j = 0, \dots, N$, we obtain Eq. (B1) for the system (B21). It follows that $\sigma = 1$.

[1] U. M. Titulaer and R. J. Glauber, Correlation functions for coherent fields, *Phys. Rev.* **140**, B676 (1965).

[2] L. Mandel, Non-classical states of the electromagnetic field, *Phys. Scr.* **T12**, 34 (1986).

[3] L. Mandel and E. Wolf, *Optical Coherence and Quantum Optics* (Cambridge University Press, Cambridge, 1995).

[4] W. Vogel and D.-G. Welsch, *Quantum Optics* (Wiley-VCH, Weinheim, 2006).

[5] G. S. Agarwal, *Quantum Optics* (Cambridge University Press, Cambridge, 2013).

[6] R. Schnabel, Squeezed states of light and their applications in laser interferometers, *Phys. Rep.* **684**, 1 (2017).

[7] J. Sperling and I. A. Walmsley, Quasiprobability representation of quantum coherence, *Phys. Rev. A* **97**, 062327 (2018).

[8] J. Sperling and I. A. Walmsley, Quasistates and quasiprobabilities, *Phys. Rev. A* **98**, 042122 (2018).

[9] J. Sperling and W. Vogel, Quasiprobability distributions for quantum-optical coherence and beyond, *Phys. Scr.* **95**, 034007 (2020).

[10] R. J. Glauber, Coherent and incoherent states of the radiation field, *Phys. Rev.* **131**, 2766 (1963).

[11] E. C. G. Sudarshan, Equivalence of semiclassical and quantum mechanical descriptions of statistical light beams, *Phys. Rev. Lett.* **10**, 277 (1963).

[12] L. Mandel, Sub-Poissonian photon statistics in resonance fluorescence, *Opt. Lett.* **4**, 205 (1979).

[13] D. Stoler, Equivalence classes of minimum uncertainty packets, *Phys. Rev. D* **1**, 3217 (1970).

[14] D. Stoler, Equivalence classes of minimum-uncertainty packets. ii, *Phys. Rev. D* **4**, 1925 (1971).

[15] L.-A. Wu, H. J. Kimble, J. L. Hall, and H. Wu, Generation of squeezed states by parametric down conversion, *Phys. Rev. Lett.* **57**, 2520 (1986).

[16] L.-A. Wu, M. Xiao, and H. J. Kimble, Squeezed states of light from an optical parametric oscillator, *J. Opt. Soc. Am. B* **4**, 1465 (1987).

[17] H. Vahlbruch, M. Mehmet, K. Danzmann, and R. Schnabel, Detection of 15 dB squeezed states of light and their application for the absolute calibration of photoelectric quantum efficiency, *Phys. Rev. Lett.* **117**, 110801 (2016).

[18] G. S. Agarwal and K. Tara, Nonclassical character of states exhibiting no squeezing or sub-Poissonian statistics, *Phys. Rev. A* **46**, 485 (1992).

[19] M. D. Reid and D. F. Walls, Violations of classical inequalities in quantum optics, *Phys. Rev. A* **34**, 1260 (1986).

[20] M. Hillery, Nonclassical distance in quantum optics, *Phys. Rev. A* **35**, 725 (1987).

[21] C. T. Lee, Measure of the nonclassicality of nonclassical states, *Phys. Rev. A* **44**, R2775 (1991).

[22] G. Agarwal, Nonclassical characteristics of the marginals for the radiation field, *Opt. Commun.* **95**, 109 (1993).

[23] D. N. Klyshko, Observable signs of nonclassical light, *Phys. Lett. A* **213**, 7 (1996).

[24] W. Vogel, Nonclassical states: An observable criterion, *Phys. Rev. Lett.* **84**, 1849 (2000).

[25] T. Richter and W. Vogel, Nonclassicality of quantum states: A hierarchy of observable conditions, *Phys. Rev. Lett.* **89**, 283601 (2002).

[26] J. K. Asbóth, J. Calsamiglia, and H. Ritsch, Computable measure of nonclassicality for light, *Phys. Rev. Lett.* **94**, 173602 (2005).

[27] T. Kiesel, W. Vogel, V. Parigi, A. Zavatta, and M. Bellini, Experimental determination of a nonclassical Glauber-Sudarshan P function, *Phys. Rev. A* **78**, 021804(R) (2008).

[28] A. Rivas and A. Luis, Nonclassicality of states and measurements by breaking classical bounds on statistics, *Phys. Rev. A* **79**, 042105 (2009).

[29] T. Kiesel and W. Vogel, Nonclassicality filters and quasiprobabilities, *Phys. Rev. A* **82**, 032107 (2010).

[30] T. Kiesel, W. Vogel, M. Bellini, and A. Zavatta, Nonclassicality quasiprobability of single-photon-added thermal states, *Phys. Rev. A* **83**, 032116 (2011).

[31] J. Sperling, W. Vogel, and G. S. Agarwal, Sub-binomial light, *Phys. Rev. Lett.* **109**, 093601 (2012).

[32] T. J. Bartley, G. Donati, X.-M. Jin, A. Datta, M. Barbieri, and I. A. Walmsley, Direct observation of sub-binomial light, *Phys. Rev. Lett.* **110**, 173602 (2013).

[33] J. Sperling, W. Vogel, and G. S. Agarwal, Correlation measurements with on-off detectors, *Phys. Rev. A* **88**, 043821 (2013).

[34] E. Agudelo, J. Sperling, and W. Vogel, Quasiprobabilities for multipartite quantum correlations of light, *Phys. Rev. A* **87**, 033811 (2013).

[35] J. Park, J. Zhang, J. Lee, S.-W. Ji, M. Um, D. Lv, K. Kim, and H. Nha, Testing nonclassicality and non-Gaussianity in phase space, *Phys. Rev. Lett.* **114**, 190402 (2015).

[36] J. Park and H. Nha, Demonstrating nonclassicality and non-Gaussianity of single-mode fields: Bell-type tests using generalized phase-space distributions, *Phys. Rev. A* **92**, 062134 (2015).

[37] A. Luis, J. Sperling, and W. Vogel, Nonclassicality phase-space functions: More insight with fewer detectors, *Phys. Rev. Lett.* **114**, 103602 (2015).

[38] A. Miranowicz, K. Bartkiewicz, A. Pathak, J. Peřina, Y.-N. Chen, and F. Nori, Statistical mixtures of states can be more quantum than their superpositions: Comparison of nonclassicality measures for single-qubit states, *Phys. Rev. A* **91**, 042309 (2015).

[39] A. Miranowicz, K. Bartkiewicz, N. Lambert, Y.-N. Chen, and F. Nori, Increasing relative nonclassicality quantified by standard entanglement potentials by dissipation and unbalanced beam splitting, *Phys. Rev. A* **92**, 062314 (2015).

[40] B. Yadin, F. C. Binder, J. Thompson, V. Narasimhachar, M. Gu, and M. S. Kim, Operational resource theory of continuous-variable nonclassicality, *Phys. Rev. X* **8**, 041038 (2018).

[41] S. Luo and Y. Zhang, Quantifying nonclassicality via Wigner-Yanase skew information, *Phys. Rev. A* **100**, 032116 (2019).

[42] J. Peřina, V. Michálek, and O. Haderka, Non-classicality of optical fields as observed in photocount and photon-number distributions, *Opt. Express* **28**, 32620 (2020).

[43] M. Bohmann and E. Agudelo, Phase-space inequalities beyond negativities, *Phys. Rev. Lett.* **124**, 133601 (2020).

[44] M. Bohmann, E. Agudelo, and J. Sperling, Probing nonclassicality with matrices of phase-space distributions, *Quantum* **4**, 343 (2020).

[45] A. A. Semenov and A. B. Klimov, Dual form of the phase-space classical simulation problem in quantum optics, *New J. Phys.* **23**, 123046 (2021).

[46] L. Innocenti, L. Lachman, and R. Filip, Nonclassicality detection from few Fock-state probabilities, *npj Quantum Inf.* **8**, 30 (2022).

[47] L. Innocenti, L. Lachman, and R. Filip, Coherence-based operational nonclassicality criteria, *Phys. Rev. Lett.* **131**, 160201 (2023).

[48] J. Fiurášek, Tight nonclassicality criteria for unbalanced Hanbury Brown-Twiss measurement scheme with click detectors, *Phys. Rev. A* **109**, 033713 (2024).

[49] V. S. Kovtoniuk, E. V. Stolyarov, O. V. Kliushnichenko, and A. A. Semenov, Tight inequalities for nonclassicality of measurement statistics, *Phys. Rev. A* **109**, 053710 (2024).

[50] S. K. Manikandan and F. Wilczek, Testing the coherent-state description of radiation fields, *Phys. Rev. A* **111**, 033705 (2025).

[51] M. Horodecki and O. Jannathan, (quantumness in the context of) resource theories, *Int. J. Mod. Phys. B* **27**, 1345019 (2013).

[52] E. Chitambar and G. Gour, Quantum resource theories, *Rev. Mod. Phys.* **91**, 025001 (2019).

[53] A. Streltsov, G. Adesso, and M. B. Plenio, Colloquium: Quantum coherence as a resource, *Rev. Mod. Phys.* **89**, 041003 (2017).

[54] W. Ge, K. Jacobs, S. Asiri, M. Foss-Feig, and M. S.

Zubairy, Operational resource theory of nonclassicality via quantum metrology, *Phys. Rev. Res.* **2**, 023400 (2020).

[55] W. Ge and M. S. Zubairy, Evaluating single-mode nonclassicality, *Phys. Rev. A* **102**, 043703 (2020).

[56] S. Rahimi-Keshari, T. C. Ralph, and C. M. Caves, Sufficient conditions for efficient classical simulation of quantum optics, *Phys. Rev. X* **6**, 021039 (2016).

[57] U. Chabaud, R. Ghobadi, S. Beigi, and S. Rahimi-Keshari, Phase-space negativity as a computational resource for quantum kernel methods, *Quantum* **8**, 1519 (2024).

[58] P. L. Kelley and W. H. Kleiner, Theory of electromagnetic field measurement and photoelectron counting, *Phys. Rev.* **136**, A316 (1964).

[59] J. Sperling, W. Vogel, and G. S. Agarwal, True photocounting statistics of multiple on-off detectors, *Phys. Rev. A* **85**, 023820 (2012).

[60] A. A. Semenov, J. Samelin, C. Boldt, M. Schüneemann, C. Reiher, W. Vogel, and B. Hage, Photocounting measurements with dead time and afterpulses in the continuous-wave regime, *Phys. Rev. A* **109**, 013701 (2024).

[61] V. A. Uzunova and A. A. Semenov, Photocounting statistics of superconducting nanowire single-photon detectors, *Phys. Rev. A* **105**, 063716 (2022).

[62] E. V. Stolyarov, O. V. Kliushnichenko, V. S. Kovtoniuk, and A. A. Semenov, Photon-number resolution with microwave Josephson photomultipliers, *Phys. Rev. A* **108**, 063710 (2023).

[63] K. E. Cahill and R. J. Glauber, Density operators and quasiprobability distributions, *Phys. Rev.* **177**, 1882 (1969).

[64] K. E. Cahill and R. J. Glauber, Ordered expansions in boson amplitude operators, *Phys. Rev.* **177**, 1857 (1969).

[65] S. Boyd and L. Vandenberghe, *Convex Optimization* (Cambridge University Press, Cambridge, England, 2004).

[66] V. S. Kovtoniuk, I. S. Yeremenko, S. Ryl, W. Vogel, and A. A. Semenov, Nonclassical correlations of radiation in relation to Bell nonlocality, *Phys. Rev. A* **105**, 063722 (2022).

[67] S. Karlin and W. Studden, *Tchebycheff Systems: With Applications in Analysis and Statistics*, Pure and Applied Mathematics: Interscience (Interscience Publishers, New York, 1966).

[68] M. G. Krein and A. A. Nudel'man, *The Markov Moment Problem and Extremal Problems*, Translations of mathematical monographs, vol. 50 (American Mathematical Society, Rhode Island, 1977).

[69] J. de Dios Pont, P. Ivanisvili, and J. Madrid, A new proof of the description of the convex hull of space curves with totally positive torsion (2023), [arXiv:2201.12932 \[math.PR\]](https://arxiv.org/abs/2201.12932).

[70] T. Frankel, *The geometry of physics: An introduction*, 3rd ed. (Cambridge University Press, Cambridge, England, 2012).